Chemistry–A European Journal

Full Paper
doi.org/10.1002/chem.202000637

Europe
European Chemical
Societies Publishing

Check for updates

■ **Nanomaterials** |*Hot Paper*|

Towards Atomically Precise Supported Catalysts from Monolayer-Protected Clusters: The Critical Role of the Support

Alessandro Longo,*[a, e] Ewoud J. J. de Boed,[b] Nisha Mammen,[c] Marte van der Linden,[b] Karoliina Honkala,[d] Hannu Häkkinen,*[c, d] Petra E. de Jongh,[b] and Baira Donoeva*[b]

Abstract: Controlling the size and uniformity of metal clusters with atomic precision is essential for fine-tuning their catalytic properties, however for clusters deposited on supports, such control is challenging. Here, by combining X-ray absorption spectroscopy and density functional theory calculations, it is shown that supports play a crucial role in the evolution of monolayer-protected clusters into catalysts. Based on the acidic nature of the support, cluster-support interactions lead either to fragmentation of the cluster into isolated Au–ligand species or ligand-free metallic Au^0 clusters. On Lewis acidic supports that bind metals strongly, the latter transformation occurs while preserving the original size of the metal cluster, as demonstrated for various Au_n sizes. These findings underline the role of the support in the design of supported catalysts and represent an important step toward the synthesis of atomically precise supported nanomaterials with tailored physico-chemical properties.

Introduction

Sub-nanometer metal clusters possess unique electronic, optical, magnetic and chemical properties.[1] These small metal clusters are particularly attractive for catalysis due to the accessibility of nearly all metal atoms to gas or liquid reactants rendering the highest possible efficiency in metal utilization.[2] In the sub-nanometer regime the properties of metal clusters are often non-scalable with their atomicity. For example, the addition/removal of a single metal atom to/from a cluster may lead to a drastic change in its properties, meaning that every metal atom in a cluster is important.[3] Examples of dramatic effects of the nuclearity on catalytic properties include oscillatory behaviour of Au clusters with even or odd number of atoms for adsorption and activation of small molecules shown for gas-phase Au clusters;[3b,c,4] activity of Au clusters only with 5–10 atoms in the oxidation of thiophenol[5] or with 3–6 atoms in coupling reactions;[6] activation of methane over gold clusters;[4d,7] remarkable difference in hydrogenation activity for carbon-supported Pt_8, Pt_9 and Pt_{10},[8] etc.[9] Furthermore, such cluster size effects in the sub-nm regime were observed even in reactions that are generally regarded as structure-insensitive.[10] In order to understand such atomic level cluster size effects, an extremely challenging control over the nuclearity and uniformity of supported clusters is required.

For most applications, including catalysis, metal nanoparticles have to be supported on a high surface area solid carrier primarily to prevent them from agglomeration. Although a number of ways to synthesize well-defined metal clusters in the gas phase or solution exist, controlling the size and uniformity of clusters on supports is extremely challenging. For example, monodisperse organometallic precursors with the desired size are deposited onto porous supports with subsequent activation at high temperature to unblock the active metal surface from organic ligands.[11] However, the latter step often leads to cluster sintering with the loss of the original size and uniformity.[12]

Currently, oxide-supported low-nuclearity carbonyl clusters of group VII–IX metals are best understood systems in terms of immobilization, interaction with supports and de-ligation.[11a–c]

[a] Dr. A. Longo
XMI, Department of Chemistry, Ghent University
Krijgslaan 281 S12, Ghent, East Flanders 9000 (Belgium)

[b] Dr. E. J. J. de Boed, Dr. M. van der Linden, Prof. Dr. P. E. de Jongh,
Dr. B. Donoeva
Department of Chemistry, Inorganic Chemistry and Catalysis
Debye Institute for Nanomaterials Science
Utrecht University, Universiteitsweg 99, 3584 CG Utrecht (The Netherlands)
E-mail: b.donoeva@uu.nl

[c] Dr. N. Mammen, Prof. Dr. H. Häkkinen
Department of Physics, Nanoscience Center
University of Jyväskylä, Jyväskylä 40014 (Finland)

[d] Prof. Dr. K. Honkala, Prof. Dr. H. Häkkinen
Department of Chemistry, Nanoscience Center
University of Jyväskylä, Jyväskylä 40014 (Finland)
E-mail: hannu.j.hakkinen@jyu.fi

[e] Dr. A. Longo
Istituto per lo Studio dei Materiali Nanostrutturati (ISMN)-CNR
UOS Palermo, Via Ugo La Malfa, 153, 90146 Palermo (Italy)
E-mail: alessandro.longo@esrf.fr

Chemistry–A European Journal

Full Paper
doi.org/10.1002/chem.202000637

Chemistry Europe
European Chemical
Societies Publishing

Cluster-support interactions are known to play a major role in the formation of active metal nanoclusters.

Monolayer-protected Au, Pt and Ag clusters have attracted a lot of interest due to the possibility to precisely control their size and composition in a uniform manner.[8, 11f,h, 13] Thiolate-protected Au clusters have been actively investigated in recent years as precursors for heterogeneous catalysts,[11g,h, 13b,g,h, 14] however less knowledge is available for the phosphine-protected atomically precise clusters.[15] For example, interaction between phosphine clusters and support materials is not fully understood and studied. Gaining a better understanding of the behaviour of metal-organic clusters on supports is of utmost importance for the design of well-defined supported nanomaterials.

Here, by employing phosphine-stabilized Au_n clusters (with $n = 1, 8, 9$) and clusters with the average size $n = 101$, and a combination of X-ray absorption spectroscopy methods and density functional theory (DFT) calculations, we have investigated the interaction between the clusters and four different supports: silica, graphitic carbon, titania and ceria. We demonstrate that these stable clusters readily react with these supports already at temperatures as low as 60 °C, undergoing fragmentation via two different mechanisms, governed solely by the surface chemistry of the support. We observe that the clusters break down by "oxidative fragmentation" into Au–PPh$_3$ species when placed on Brønsted acidic supports such as silica and oxidized graphitic carbon, while on Lewis acidic supports such as titania and ceria, the clusters break down by "ligand migration" into metallic Au_n clusters and PPh$_3$ species on the surface of the support.

Au/CeO$_2$ catalysts show high activity in the oxidation of CO, water–gas shift, selective oxidation and other reactions.[17] Here, we report the catalytic activity of the well-defined Au_n clusters formed after ligand migration on the CeO$_2$ surface in the oxidation of carbon monoxide and show that the size of Au_n clusters significantly affects the catalytic activity. These insights open new strategies for designing atomically precise, monodisperse, supported heterogeneous catalysts that can take advantage of the size-dependent properties of the metal clusters for controlling catalytic reactions.

Results and Discussion

Cluster immobilization on supports at ambient temperature

We have performed experiments and analysis for Au_n clusters; $n = 1, 8, 9$ and 101, however, here we focus on the results for $n = 9$ and show our results for $n = 1, 8$ and 101 in the Supporting Information. The clusters for $n = 1, 8, 9$ and 101, correspond to AuL(NO$_3$), Au$_8$L$_8$(NO$_3$)$_2$, Au$_9$L$_8$(NO$_3$)$_3$ and Au$_{101}$L$_x$(NO$_3$)$_y$, respectively, where L = PPh$_3$. These clusters are deposited on four different supports, SiO$_2$, TiO$_2$, CeO$_2$ and oxidized graphitic carbon (for the latter support only data for the thermally treated sample was recorded). Note that the NO$_3^-$ counter-anions are washed away during the sample treatment, before characterization. Table 1 shows surface acid characteristics. SiO$_2$ and graphitic carbon contain only Brønsted acid sites with silanols[11c] on SiO$_2$ or carboxylic, lactonic and hydroxyl groups[18] on carbon. TiO$_2$, in addition to the low density of Brønsted acid sites, also shows Lewis acidity, while CeO$_2$ has only Lewis acid sites.

Table 1. Support Lewis/Brønsted acid characteristics.

Support	Point of zero charge	Brønsted acid sites [nm^{-2}][a]	Lewis acid sites [nm^{-2}][a]
SiO$_2$	4.1	0.2	–
Carbon	4.0	0.16[18][b]	–
TiO$_2$	3.8	0.003	0.74
CeO$_2$	4.4	–	0.21

[a] determined from Pyridine-IR (Figure S2). [b] Determined by acid–base titration.

Figure 1a shows the structure of the unsupported [Au$_9$L$_8$]$^{3+}$ cluster. The cluster has an icosahedral positively charged Au core of around 1 nm with NO$_3^-$ as a counter-ion and a formal charge on each Au atom of +0.3. (electrospray ionization mass spectra and transmission electron microscopy image of the unsupported cluster are shown in Figure S1. Figure S5 shows the structure of the unsupported [Au$_8$L$_8$]$^{2+}$ cluster and further structural characteristics of $n = 1, 8$ and 9 clusters are listed in Table S1 in the Supporting Information). Phosphines are L-type ligands that bind to Au via a dative interaction, where PPh$_3$ acts as a Lewis base due to the lone pair of electrons on P, and Au acts as a Lewis acid.[19]
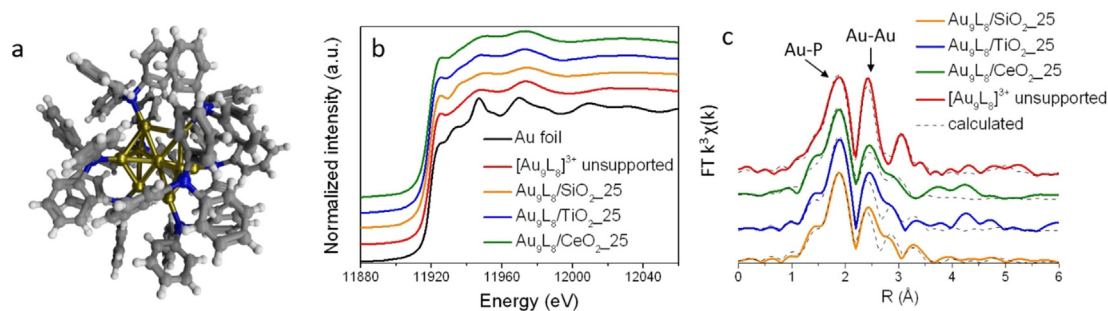

Figure 1. (a) Structure of [Au$_9$(PPh$_3$)$_8$]$^{3+}$;[16] (b) Au L$_{III}$ XANES and (c) Fourier transformation of the EXAFS spectra of [Au$_9$L$_8$]$^{3+}$ unsupported and when supported on oxides dried at 25 °C. The FT spectra are uncorrected for the phase shift.

Chemistry–A European Journal

Full Paper
doi.org/10.1002/chem.202000637

Chemistry
Europe
European Chemical
Societies Publishing

Figure 1 b shows the X-ray absorption near edge structure (XANES) spectra for the unsupported cluster (red), supported clusters and a metallic Au foil (black). The peak at around 11 920 eV ("white line") seen for the unsupported $[Au_9L_8]^{3+}$, and different oxide-supported $[Au_9L_8]^{3+}$ dried at 25 °C (denoted Au_9L_8/MO_2_25) confirms the positive charge on gold in these samples.

Figure 1 c shows the Fourier transform (FT) analysis of the Au L_{III}-edge extended X-ray absorption fine structure (EXAFS). For the unsupported $[Au_9L_8]^{3+}$ (red), peaks due to Au–P and Au–Au bonds are observed at 2.28 and 2.7–3.1 Å, respectively, with both coordination numbers (CN) being one (Tables 2 and

Table 2. Structural characteristics of Au_9L_8 clusters on various supports dried at ambient and elevated temperature based on curve fitting analysis of Au L_{III}-edge EXAFS (see k^3-weighted spectra in the Supporting Information).

Catalyst	Bond	CN[a]	r [Å][b]	$\Delta\sigma^{2[c]}$ 10⁻¹³
Au_9L_8/SiO_2_25	Au–Au	2.2 (6)[d]	2.71 (6)	2.5 (3)
	Au–P	0.8 (5)	2.32 (1)	1.9 (3)
Au_9L_8/CeO_2_25	Au–Au	3.0 (5)	2.69 (1)	1.6 (3)
	Au–P	0.8 (2)	2.29 (2)	1.0 (1)
Au_9L_8/TiO_2_25	Au–Au	2.3 (5)	2.71 (5)	2.6 (3)
	Au–P	1.0 (3)	2.28 (3)	1.5 (2)
AuL/SiO_2_120	Au–Au	1.2 (5)	3.01 (3)	4.1 (4)
	Au–P/Au–O	1.6 (3)	2.23 (3)	8.4 (4)
Au_9/CeO_2_120	Au–Au	4.5 (5)	2.83 (3)	4.1 (5)
	Au–O	0.5 (2)	2.23 (5)	1.2 (3)
Au_n/TiO_2_120	Au–Au	7.8 (2)	2.86 (5)	3.2 (2)
	Au–P/Au–O	–	–	–
$AuL/Carbon\_60$	Au–Au	1.0 (1)	3.41 (3)	6.0 (7)
	Au–P/Au–O	1.8 (3)	2.19 (5)	6.0 (2)

[a] CN coordination number. [b] Bond length. [c] Relative Debye–Waller factor: $\sigma^2 = (\sigma_{sample})^2$. [d] Number ($x$) in brackets indicates a standard deviation of ±0.x to the value before it.

S1). The Au–Au CN is lower than expected for a cluster of 9 atoms. The underestimation of Au–Au CN is known for monolayer-protected clusters and arises from their disordered low-symmetry structures.[13b, 14a] Our DFT calculated value for the average Au–P bond length is 2.37 Å and Au–Au lengths range between 2.86–3.02 Å, for the $[Au_9L_8]^{3+}$ cluster in gas phase, in good agreement with the experimental values. The spectra of $[Au_9L_8]^{3+}$ and Au_9L_8/MO_2_25 are similar with only small differences in the Au–Au bond region. This suggests that on all three supports considered here, the deposited $[Au_9L_8]^{3+}$ clusters remain essentially unaltered and retain their core structure, the PPh_3 ligands and positive charge on gold when deposited on supports followed by drying at ambient temperature.

Oxidative fragmentation of gold-phosphine clusters on Brønsted acidic supports

We show that $[Au_9L_8]^{3+}$ clusters supported on Brønsted acid supports, such as SiO_2 and carbon, undergo oxidative fragmentation and disintegrate into ensembles of $Au-PPh_3$ (AuL) frag-

ments upon heating to temperatures of 120 °C on SiO_2 (AuL/SiO_2_120) and 60 °C on graphitic carbon (AuL/Carbon_60). This result is evidenced by several observations that we describe below.

Figure 2 a shows the UV/Vis spectra of the unsupported $[Au_9L_8]^{3+}$ (in methanol), and Au_9L_8 supported on SiO_2 at 25 and 120 °C. The optical absorption features characteristic of the unsupported $[Au_9L_8]^{3+}$ (in methanol), are also seen for Au_9L_8/SiO_2_25 but they disappear upon heating the system to 120 °C. This clearly indicates that $[Au_9L_8]^{3+}$ clusters on SiO_2 undergo a structural change. Similar result for $n=8$ cluster is shown in Figure S6. (Due to the band gap peak of the semiconductor supports (CeO_2 and TiO_2) or a complete light absorption on a carbon-supported catalyst, the changes in the UV–visible spectra of the supported cluster upon thermal treatment were not as pronounced on other supports as on SiO_2).

The FT EXAFS spectra in Figure 2 b show that after thermal treatment the peaks due to Au–Au bonds in the original $[Au_9L_8]^{3+}$ cluster (red curve) are absent in AuL/SiO_2_120 (orange curve) and AuL/Carbon_60 (pink curve), and only a small Au–Au bond peak is observed at 3.4 Å, suggesting that Au–Au bonds have broken. Furthermore, we also show that the FT EXAFS of both supported samples are very similar to that of the isolated $AuPPh_3NO_3$ complex (light green curve) in Figure 2 b. This strongly suggests the fragmentation of Au_9L_8 clusters into AuL species.

We provide additional support in Figure 2 c, where we show that the shape of the white line in the XANES spectra of AuL/SiO_2_120 and AuL/Carbon_60 is similar to that of $AuPPh_3NO_3$. The formal oxidation state of Au in $AuLNO_3$ is +1. The similarity between the XANES features of the samples and $[AuL]^{1+}$ suggests the same charge of +1 on Au. Hence, the thermal evolution of $[Au_9L_8]^{3+}$ on SiO_2 and carbon is accompanied by an increase in the formal oxidation state of Au from +0.3 to +1.

Unsupported $[Au_9L_8]^{3+}$ clusters are stable up to 250 °C under both oxidizing and reducing conditions (gravimetric analysis shown in Figure S3), therefore the observed fragmentation of $[Au_9L_8]^{3+}$ clusters at a considerably lower temperature (<120 °C) is the result of their chemical interaction with the Brønsted acid surface groups on SiO_2 and oxidized graphitic carbon. Hence, by analogy with molecular acids, the hydroxyl groups on SiO_2 or carboxylic groups on carbon oxidize gold in $[Au_9L_8]^{3+}$ clusters to yield surface-bound L-Au-O-Si/C complexes. On acidic carbon, clusters fully fragment already at 60 °C (cf. 120 °C for SiO_2) likely due to the higher Brønsted acid strength of the carboxylic groups on carbon relative to that of hydroxyls on SiO_2.

The formation of support-bound L-Au-O-Si/C complexes is evidenced by the increase in the Au-P/O coordination number relative to the unsupported clusters: in $[Au_9L_8]^{3+}$ and $[AuL]^{1+}$ the Au-P CN is found to be 1, while in AuL/SiO_2_120 and AuL/Carbon_60, it increases to 1.6 and 1.8, respectively. This is also supported by the shortened average Au–P/O bond length due to the contribution from the shorter Au–O bond (Tables 2 and S1). The presence of the Au–Au bond peak at 3.4 Å, that is, at non-bonding distances, for AuL/SiO_2_120 and AuL/Carbon_60

Chemistry–A European Journal

Full Paper
doi.org/10.1002/chem.202000637

Chemistry
Europe
European Chemical
Societies Publishing
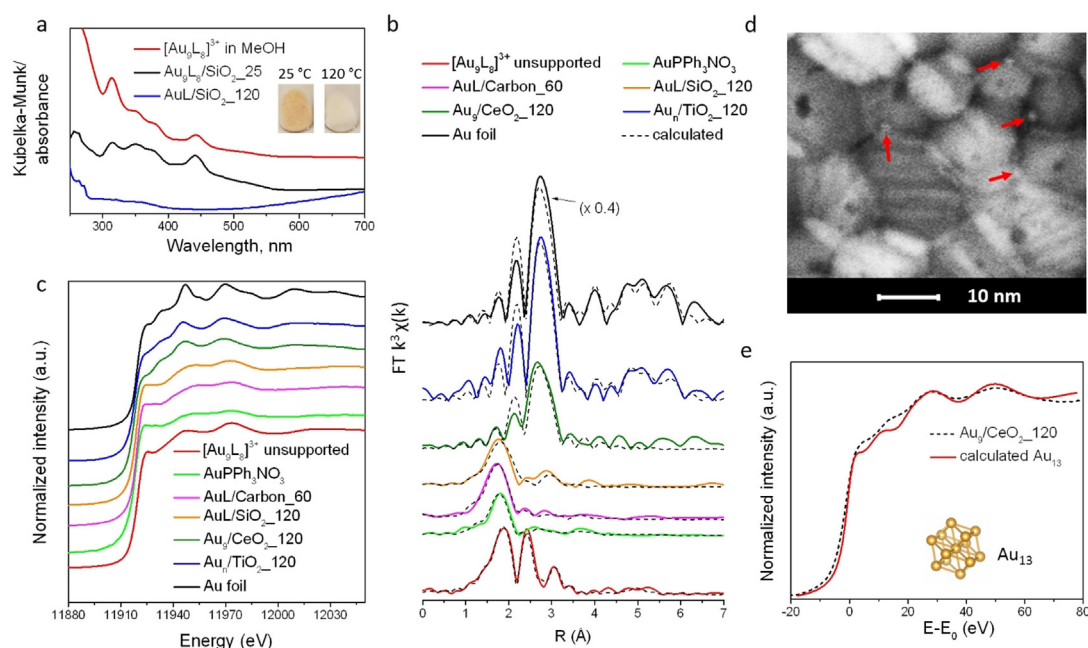
Figure 2. (a) UV/Vis of the unsupported $[Au_9L_8]^{3+}$ in methanol, DR UV/Vis and photographs (inset) of Au_9L_8/SiO_2_25 and AuL/SiO_2_120. (b) FT of Au L_{III} EXAFS (uncorrected for the phase shift) and (c) Au L_{III} XANES of supported $[Au_9L_8]^{3+}$ (at total Au loading 0.2 wt.%, see Table 3) after thermal treatment and reference compounds. FT EXAFS intensity of Au foil was reduced 2.5 times to fit in the Figure. (d) HAADF-STEM of Au_9/CeO_2_120. Au nanoclusters are seen as white dots. (e) Experimental Au L_{III} XANES of Au_9/CeO_2_120 and calculated XANES of Au_{13}.

shows that the Au-phosphine complexes exist on the supports as ensembles, similar to isolated Au^I-phosphine complexes that tend to form dimers/polymers due to aurophilic Au—Au interactions.[20]

This oxidative fragmentation of phosphine-protected Au clusters aided by the Brønsted acidic groups of the supports is similar to the behaviour of carbonyl clusters of more oxophilic metals of Groups VII–IX (e.g. Ir, Rh, Os, Re).[11c] Unlike phosphine stabilized Au clusters, the more reactive metal carbonyl clusters were shown to react with metal oxide surfaces already upon chemisorption, and fragment at elevated temperatures with the evolution of H_2 and CO, confirming oxidative addition of surface hydroxyls to metal.[11c, 21] It is hence intriguing that the rather inert phosphine-protected Au clusters react with the Brønsted acidic groups of supports at elevated temperature in a similar manner as metal carbonyls.

Ligand migration from gold-phosphine clusters to Lewis acidic supports

In contrast to the behaviour of the $[Au_9L_8]^{3+}$ clusters on Brønsted acid supports, on Lewis acid supports, such as CeO_2 and TiO_2, upon heating to a temperature of 120 °C, the ligands migrate from the cluster to the Lewis acid sites on the support leaving behind ligand-free metallic Au_n clusters on the surface. On CeO_2, the Au_9 cluster seems to maintain its size ($Au_9/CeO_2\_$ 120), while on TiO_2, the cluster is found to agglomerate to form somewhat larger Au_n clusters (Au_n/TiO_2_120).

FT EXAFS of both samples indicate complete migration of phosphine ligands from gold evidenced by the absence of the Au-P bond peak (Figure 2b and Table 2). The metallic state of

Au in Au_9/CeO_2_120 and Au_n/TiO_2_120 is evidenced by the absence of the white line in the XANES spectra in Figure 2c. The spectra seem similar now to the spectrum of the metallic Au foil. The XANES and FT EXAFS spectra for $n=1$ and 8 clusters on CeO_2 are shown in Figure S7. The structural characteristics of $n=1$, 8 and 101 clusters on CeO_2 are listed in Table S2. These results suggest that migration of the phosphine ligands to CeO_2, while preserving the original cluster size, occurs irrespective of the size of the cluster.

For Au_9/CeO_2, the Au—Au coordination number increased to 4.5 and Au—Au bonds elongated to 2.83 Å upon heating to 120 °C, thus indicating the rearrangement of the Au core with equalization of the Au—Au bond length (Figure 2b, Table 2). Figure 2d shows the HAADF-STEM of Au_9/CeO_2_120 with Au clusters of 1 nm in agreement with the size of the unsupported $[Au_9L_8]^{3+}$ (Figure S1). For an icosahedral or cuboctahedral cluster of 13 atoms, the expected CN lie in the range of 5.5–6.5.[22] Hence, the short Au—Au bond (2.83 Å),[23] the absence of the higher shell Au—Au bonds with distances above 4 Å, and the low Au—Au CN (4.5) for Au_9/CeO_2_120 show that the resulting phosphine-free Au clusters on ceria are very small and the majority of clusters maintain the original size of 9 atoms with negligible sintering, if any. Furthermore, a comparison of the experimental XANES of Au_9/CeO_2_120 and simulated XANES of a model Au_{13} cluster (see Figure 2e) shows that XANES features are less pronounced for Au_9/CeO_2_120, which supports our conclusion that the average cluster size in this sample is not higher than 13 atoms.[24]

On TiO_2, phosphine-free Au^0 clusters sinter to form larger particles as evidenced by the increased Au—Au CN (7.8), larger Au—Au bond lengths of 2.86 Å and the appearance of the

Chemistry–A European Journal | Full Paper
doi.org/10.1002/chem.202000637

**Chemistry
Europe**
European Chemical
Societies Publishing

higher shell Au–Au bond peaks at 4–7 Å (Figure 2b, Table 2). The cluster size is preserved on CeO_2 likely due to its higher number of surface defects (oxygen vacancies) and stronger metal adhesion compared to TiO_2.[25] We note that electronic properties of CeO_2 in Au_9/CeO_2_120 in the vicinity of gold clusters are probably altered due to interaction with phosphine ligands (vide infra).

What causes the loss of phosphine ligands from gold clusters? P1s X-ray photoelectron spectroscopy (XPS) shows that phosphine species are present in Au_9/CeO_2_120 (see Figure S4) therefore they must reside on the support. Phosphine species function as Lewis bases and form dative bonds to Lewis acid sites (under-coordinated Ti^{4+} and Ce^{4+}) on TiO_2 and CeO_2.[26] Therefore, the stronger interaction of the phosphines with the Lewis acid sites compared to the interaction with Au is the reason for the observed ligand migration from the clusters to the support. TiO_2 and CeO_2 surfaces are both hydroxylated,[27] and TiO_2 used in this work shows weakly Brønsted acidic properties (point of zero charge of ca. 3.8, Table 1), however no Au cluster fragmentation occurs on these supports. This suggests that the presence of Lewis acid sites determines the specific pathway for the evolution of these clusters when both Brønsted and Lewis acid groups co-exist on the support surface. This reasoning is also supported by our DFT calculations described below.

Oxidative fragmentation vs. migration of ligands of $[Au_9L_8]^{3+}$ clusters on supports: DFT analysis

To investigate the thermodynamic driving forces behind the interactions of the $[Au_9L_8]^{3+}$ cluster with Brønsted acid and Lewis acid surfaces, we resort to density functional theory (DFT) calculations. We study the interaction of the cluster with hydroxylated amorphous silica ($HO-SiO_2$) and hydroxylated ceria (111) ($HO-CeO_2$) surfaces; on both supports, we consider the two mechanisms: (1) oxidative fragmentation into AuL species and (2) ligand migration forming Au_9 and L species on the supports.

In the first case, the $[Au_9L_8]^{3+}$ cluster breaks down into eight AuL species each removing a hydrogen from one of the surface hydroxyl groups thereby forming $L-Au-O-MO_2$; M = Si/Ce. The remaining Au in the $[Au_9L_8]^{3+}$ cluster also removes a H from a hydroxyl group and forms $Au-O-MO_2$. Equation (1) shows the considered reaction:

$$[Au_9L_8]^{3+} + 9\ HO\text{-}MO_2 \rightarrow 8\ L\text{-}Au\text{-}O\text{-}MO_2 + Au\text{-}O\text{-}MO_2 + 9/2\ H_2$$

(1)
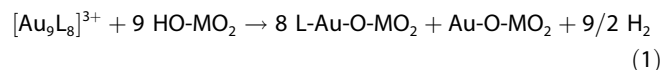
Note that this equation is formally charge-imbalanced. However, we have implicitly taken into account the enthalpy contribution to reduce the $[Au_9L_8]^{3+}$ in the left-hand side of Eq. (1) by performing calculations in a Born–Haber cycle (to be shown later). The lowest energy configurations obtained by DFT for the species $L-Au-O-MO_2$ and $Au-O-MO_2$ for M = Si are shown in Figures 3a,b, respectively, while those for M = Ce are shown in Figures 3e,f, respectively.
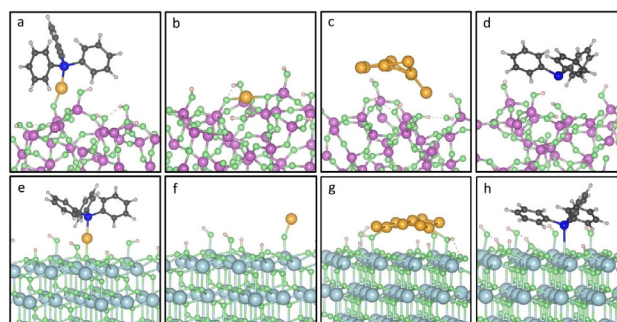

Figure 3. Lowest energy geometries obtained from DFT for different species on hydroxylated amorphous silica and hydroxylated ceria (111) surfaces. (a)–(d) AuL and Au species formed by oxidative fragmentation, and Au_9 and L formed by ligand migration, respectively on the SiO_2 surface. (e)–(h) AuL and Au species formed by oxidative fragmentation, and Au_9 and L formed by ligand migration, respectively on the CeO_2 surface. Au, P, C, O, Si and Ce are shown by yellow, blue, dark grey, pale green, pink and pale blue colours, respectively. H atoms in the phenyl ring and on the surface hydroxyl groups are shown by light grey and light pink colours, respectively.

In the second case, the $[Au_9L_8]^{3+}$ cluster breaks down into metallic Au_9 and L species. The Au_9 cluster adsorbs on the support by interacting with surface O atoms, while the ligand L forms a dative bond with the cation in the oxide. The reaction (formally charge-imbalanced, see above) can be written as in Equation (2):

$$[Au_9L_8]^{3+} + 9\ HO\text{-}MO_2 \rightarrow Au_9/HO\text{-}MO_2 + 8\ L/HO\text{-}MO_2$$

(2)
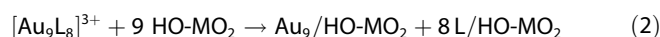
The lowest energy configurations obtained for Au_9 and L species on $HO-SiO_2$ are shown in Figures 3c,d, respectively, while those on $HO-CeO_2$ are shown in Figures 3g,h, respectively.

We show the energetics for the two mechanisms on both supports in Figure 4. The top panel (a) describes oxidative fragmentation of the $[Au_9L_8]^{3+}$ cluster into AuL species by removal of hydrogen from the surface. The reaction enthalpy for the complete reaction is given by ΔH_{tot} and is calculated to be -9.20 eV and -10.26 eV, for $HO-SiO_2$ and $HO-CeO_2$, respectively. The energy contributions to the reaction enthalpy can be split into three parts in this case: $\Delta H_{tot} = \Delta H_{rd} + 9\Delta H_{rh} + \Delta H_{int}$, where ΔH_{rd} is the energy to reduce and disintegrate the cluster into AuL species in gas phase, ΔH_{rh} is the energy to remove a neutral H atom from a hydroxyl group on the surface and ΔH_{int} is the energy due to the interaction between the disintegrated fragments and the surface after removal of H. ΔH_{rh} for both surfaces were calculated for the geometries of $O-MO_2$ that correspond to the lowest energy geometry obtained for $L-Au-O-MO_2$.

The second panel (b) in Figure 4 describes ligand migration from the $[Au_9L_8]^{3+}$ cluster to the surface, leaving behind metallic Au_9. The reaction enthalpy, ΔH_{tot}, for the reaction on the two surfaces is calculated to be -5.44 and -11.62 eV for the $HO-SiO_2$ and $HO-CeO_2$ surfaces, respectively. In this case, the energy contributions to the reaction enthalpy is split into two parts: $\Delta H_{tot} = \Delta H_{rp} + \Delta H_{int}$, where ΔH_{rp} is the energy to reduce and peel the ligands from the Au_9 cluster in gas phase and

Chemistry–A European Journal

Full Paper
doi.org/10.1002/chem.202000637

Chemistry
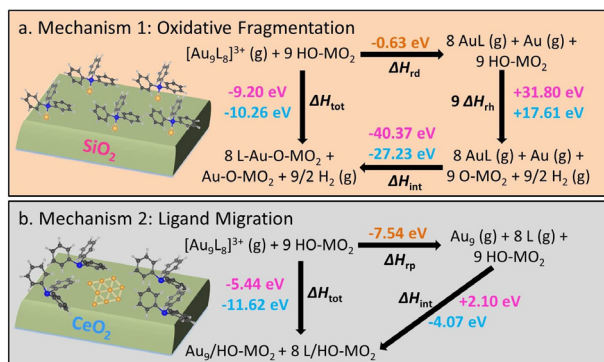Europe
European Chemical
Societies Publishing

Figure 4. The Born–Haber cycle for (a) oxidative fragmentation and (b) ligand migration for the two supports, HO-SiO$_2$ and HO-CeO$_2$. All numbers in pink correspond to values for the hydroxylated amorphous SiO$_2$ surface, while the numbers in blue correspond to energy values for the hydroxylated CeO$_2$ (111) surface. ΔH_{tot} is the total reaction enthalpy for the processes, ΔH_{rd} is the energy to reduce and disintegrate the cluster into AuL species in gas phase, ΔH_{rp} is the energy to reduce and peel the ligands from the cluster forming Au$_9$ and L species in gas phase, ΔH_{rh} is the energy to remove a H atom from the surface and ΔH_{int} is the energy due to the interaction between the end species and the surface. Note that the Born–Haber cycle implicitly takes into account the charge imbalance in the total reaction enthalpy ΔH_{tot}.

ΔH_{int} is the interaction energy between the disintegrated fragments, Au$_9$ and eight L, with the surface.

By comparing the total reaction enthalpies for the two mechanisms on silica, -9.20 eV for oxidative fragmentation vs. -5.44 eV for ligand migration, we find that DFT supports the experimental observation: there is a driving force for the surface-cluster interaction to form AuL species. Note that we assume here that the entropy contributions are similar for both mechanisms. By comparing the energetics for the disintegration of the cluster in gas phase, we see that [Au$_9$L$_8$]$^{3+}$ energetically prefers to reduce and peel the ligands forming Au$_9$ and L (-7.54 eV) than to reduce and disintegrate forming AuL species (-0.63 eV). However, the formation of Au$_9$ and L on SiO$_2$ is not favoured due to the endothermic interaction ($+2.10$ eV) between the species and the silica surface. The Au$_9$ cluster binds weakly to the surface with a binding strength of -0.12 eV with respect to Au$_9$ in gas phase and the bare support, however the binding of PPh$_3$ on the surface is unfavourable with an endothermic binding energy of $+0.28$ eV, calculated with respect to PPh$_3$ in gas phase and the bare support. This is expected on a surface such as SiO$_2$. The Si atoms are already four-coordinated and do not interact with the ligand species. The formation of the AuL and Au species, however, is highly favoured on this surface due to the high interaction energy between AuL and O-SiO$_2$. Thus, the silica surface induces the breaking of Au–Au bonds and the formation of O-Au-L bonds.
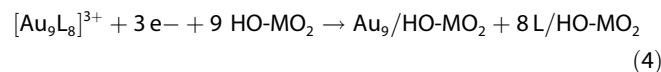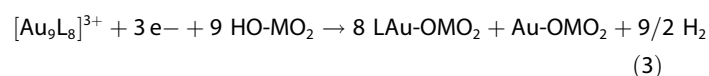
Similarly, when comparing the total reaction enthalpies for the two mechanisms on ceria: -10.26 eV for oxidative fragmentation and -11.62 eV for ligand migration, we see that again, DFT supports the experimental observation that the [Au$_9$L$_8$]$^{3+}$ cluster interacts with the surface to form Au$_9$ and L species. The energy to reduce and peel the ligands is highly

exothermic (-7.54 eV) and the fragments bind favourably to the surface (-4.07 eV). DFT suggests that the Au$_9$ cluster would have tendency to further decompose to 9 Au atoms bound on the surface (the calculated enthalpy is -4.06 eV with respect to the Au$_9$ cluster deposited on ceria). This is not observed in the experiments however, indicating that a kinetic barrier prevents this process. On the other hand, the oxidative fragmentation to AuL complexes bound to the surface requires the removal of H from the surface hydroxyl groups, which costs considerable energy. The binding strengths for the adsorption of Au$_9$ and the L on the HO-CeO$_2$ surface are calculated to be -1.76 and -0.29 eV, respectively, calculated with respect to the corresponding species in gas phase. The ceria surface favours the breaking of Au–P bonds and formation of P—Ce bonds.

Interestingly, the fragmentation of the cluster on the support is possible only in the presence of the ligands bound to gold. The energetics for oxidative fragmentation of an Au$_9$ cluster into Au atoms on the two surfaces is described in Figure S8. The considered reaction is Au$_9$ + 9 HO-MO$_2$ → 9 Au-O-MO$_2$ + 9/2 H$_2$. The reaction enthalpy, ΔH_{tot}, for the reaction on the HO-SiO$_2$ and HO-CeO$_2$ surfaces, is calculated to be $+14.60$ and $+20.60$ eV, respectively. The process is highly unfavourable. The fragmentation of the [Au$_9$L$_8$]$^{3+}$ cluster is favoured on HO-SiO$_2$, in the presence of the ligands, only due to the high binding strength of the O-Au-L bond, which is calculated to be -4.57 eV, with respect to the [AuL]^0 in gas phase and O-SiO$_2$ (after H is removed).

In Figure S9, we show energetics for the interaction between the $n=1$ cluster, [AuL]$^{1+}$, and two surfaces. On HO-SiO$_2$, the reaction enthalpies for oxidative binding and ligand migration are -6.35 and -4.00 eV, respectively, suggesting that the cluster prefers to bind to the surface forming L-Au-O-SiO$_2$ species. While on HO-CeO$_2$, the reaction enthalpies for oxidative binding and ligand migration are -6.57 and -6.88 eV, respectively supporting the finding that the ligand migrates from the Au atom to form Au adatoms and L species on the surface.

As an alternative approach to the one used in Eqs. (1) and (2), and Figure 4, one can explicitly introduce the charge balance by considering the enthalpy of the reactions (3) and (4):

$$[Au_9L_8]^{3+} + 3\,e- + 9\,HO\text{-}MO_2 \rightarrow 8\,LAu\text{-}OMO_2 + Au\text{-}OMO_2 + 9/2\,H_2 \tag{3}$$

$$[Au_9L_8]^{3+} + 3\,e- + 9\,HO\text{-}MO_2 \rightarrow Au_9/HO\text{-}MO_2 + 8\,L/HO\text{-}MO_2 \tag{4}$$

Here, we define the chemical potential of an electron (μ_e) as the energy to take an electron from the valence band of the oxide support to the lowest unoccupied molecular orbital (LUMO) of the [Au$_9$L$_8$]$^{3+}$ cluster in gas phase. The μ_e values were calculated to be -0.65 and -1.99 eV, for the supports HO-SiO$_2$ and HO-CeO$_2$, respectively. These energies were calculated after referencing the Kohn–Sham energies of the valence band of the surface and LUMO of the cluster, with respect to the same vacuum energy. Using this approach, we calculate

Chemistry–A European Journal

Full Paper
doi.org/10.1002/chem.202000637

Chemistry Europe
European Chemical
Societies Publishing

the total reaction enthalpies for Eqs. (3) and (4) for the two surfaces and find the following. On $HO-SiO_2$, the enthalpies for the two processes are -7.24 and -3.48 eV, respectively, suggesting once again that oxidative fragmentation is the preferred disintegration mechanism on $HO-SiO_2$. On the other hand, on $HO-CeO_2$, the enthalpies for the two processes are -4.30 and -5.66 eV, respectively, suggesting that ligand migration is the preferred mechanism on $HO-CeO_2$.

Effect of the Au cluster nuclearity in CO oxidation catalysis

Au_n/CeO_2_120 systems with $n = 1, 8, 9, 101$, obtained after the migration of the phosphine ligands, were tested for their catalytic activity toward the oxidation of carbon monoxide. CO oxidation over Au catalysts depends on many parameters, such as Au particle size, oxidation state, nature of the support and presence of water.[28] The activity of our Au_n/CeO_2_120 catalysts (see Table 3) increased in the order: $Au_1 < Au_8 < Au_9 < Au_{101}$, in line with previous findings.[28a,29] The activity of the phosphine Au cluster-derived Au_n/CeO_2 is lower compared to values reported for Au/CeO_2 catalysts prepared using more traditional methods, which could be related to the small size of the Au clusters in Au_n/CeO_2, and the presence of PPh_3 ligands bound to the surface around the Au clusters. The PPh_3 may hamper oxygen supply from the support and/or efficient contact between Au and the support, thus leading to a lower catalytic activity than that observed for the conventionally prepared Au/CeO_2 catalysts. As described in the previous section, ligand migration leads to the formation of the metallic Au_8 and Au_9 clusters on CeO_2 upon heating to 120 °C. Interestingly, we find that the catalytic activity of Au_9/CeO_2 is 2.2 times higher that of Au_8/CeO_2 (Table 3). This difference is substantial considering that these clusters differ by only one atom.

Au clusters with even or odd number of atoms are predicted to display the so called "even–odd oscillations" in their properties as a result of having closed- or open-shell electronic structure, respectively.[3a,30] The electronic structure of a cluster has a direct impact on the binding and activation of small molecules, such as O_2 and CO.[3a,30] Hence, we link the observed difference in catalytic activity between Au_8/CeO_2 and Au_9/CeO_2 to the different electronic structure of Au_8 and Au_9 clusters.

Conclusions

We demonstrate that supports are highly reactive towards otherwise stable monolayer-protected atomically precise clusters under very mild conditions. The properties of the support determine the type of cluster-support interaction, which ultimately defines the type of the evolving metal species. The phosphine-stabilized Au clusters deposited on different supports evolve according to two distinct pathways: a) oxidative fragmentation into ensembles of surface-bound monoatomic Au–phosphine complexes upon interaction with Brønsted acid sites on a support; b) formation of ligand-free Au^0 clusters due to the interaction of the ligands with Lewis acid sites on the support. On supports that bind metals strongly, such as CeO_2, the formation of phosphine-free Au^0 clusters occurs without a change in the original cluster size, thus enabling control over the size of supported metal clusters by tuning the size of the metal-organic precursor. Preliminary tests for the reactivity of these atomically precise clusters show that a difference in size of even one Au atom has a large impact on their catalytic activity. Our findings highlight the importance of cluster–support interactions for the design of well-defined materials and catalysts using monolayer-protected clusters. Study of these atomically precise supported clusters combined with theoretical work is expected to further advance our understanding of catalytic processes at the atomic level.

Acknowledgements

Conflict of interest

The authors declare no conflict of interest.

Table 3. Catalytic activity of Au_n/CeO_2 in the oxidation of CO at 120 °C.

Catalyst	Au loading [wt.%]	$TOF_{Au\ surf}$ [s^{-1}][a]	$TOF_{Au\ total}$ [s^{-1}][b]
Au_1/CeO_2	0.14	0.009	0.009
Au_8/CeO_2	0.24	0.025	0.025
Au_9/CeO_2	0.15	0.055	0.055
Au_{101}/CeO_2	0.16	0.066	0.051

[a] TOF normalized per surface Au sites. For Au_1, Au_8 and Au_9 clusters, all atoms were assumed to be accessible to reactants; while for Au_{101} a dispersion of 78% was used for TOF calculation. [b] TOF normalized per total Au.

[1] a) M. Walter, J. Akola, O. Lopez-Acevedo, P. D. Jadzinsky, G. Calero, C. J. Ackerson, R. L. Whetten, H. Grönbeck, H. Häkkinen, *P. Natl. Acad. Sci.*

Chemistry–A European Journal

Full Paper
doi.org/10.1002/chem.202000637

Chemistry Europe
European Chemical
Societies Publishing

USA **2008**, *105*, 9157–9162; b) Y. Lu, W. Chen, *Chem. Soc. Rev.* **2012**, *41*, 3594–3623; c) A. Sanchez, S. Abbet, U. Heiz, W. D. Schneider, H. Häkkinen, R. N. Barnett, U. Landman, *J. Phys. Chem. A* **1999**, *103*, 9573–9578.

[2] A. Wong, Q. Liu, S. Griffin, A. Nicholls, J. R. Regalbuto, *Science* **2017**, *358*, 1427.

[3] a) A. P. Woodham, G. Meijer, A. Fielicke, *Angew. Chem. Int. Ed.* **2012**, *51*, 4444–4447; *Angew. Chem.* **2012**, *124*, 4520–4523; b) B. Yoon, H. Häkkinen, U. Landman, *J. Phys. Chem. A* **2003**, *107*, 4066–4071; c) N. Veldeman, P. Lievens, M. Andersson, *J. Phys. Chem. A* **2005**, *109*, 11793–11801.

[4] a) B. E. Salisbury, W. T. Wallace, R. L. Whetten, *Chem. Phys.* **2000**, *262*, 131–141; b) L. M. Molina, B. Hammer, *J. Chem. Phys.* **2005**, *123*, 161104; c) A. Franceschetti, S. J. Pennycook, S. T. Pantelides, *Chem. Phys. Lett.* **2003**, *374*, 471–475; d) D. M. Cox, R. Brickman, K. Creegan, A. Kaldor, *Z. Phys. D* **1991**, *19*, 353–355.

[5] A. Corma, P. Concepción, M. Boronat, M. J. Sabater, J. Navas, M. J. Yacaman, E. Larios, A. Posadas, M. A. López-Quintela, D. Buceta, E. Mendoza, G. Guilera, A. Mayoral, *Nat. Chem.* **2013**, *5*, 775.

[6] J. Oliver-Meseguer, A. Leyva-Pérez, A. Corma, *ChemCatChem* **2013**, *5*, 3509–3515.

[7] X. Cai, G. Saranya, K. Shen, M. Chen, R. Si, W. Ding, Y. Zhu, *Angew. Chem. Int. Ed.* **2019**, *58*, 9964–9968; *Angew. Chem.* **2019**, *131*, 10069–10073.

[8] T. Imaoka, Y. Akanuma, N. Haruta, S. Tsuchiya, K. Ishihara, T. Okayasu, W.-J. Chun, M. Takahashi, K. Yamamoto, *Nat. Commun.* **2017**, *8*, 688.

[9] J. Oliver-Meseguer, J. R. Cabrero-Antonino, I. Domínguez, A. Leyva-Pérez, A. Corma, *Science* **2012**, *338*, 1452.

[10] A. M. Argo, J. F. Odzak, B. C. Gates, *J. Am. Chem. Soc.* **2003**, *125*, 7107–7115.

[11] a) J. Guzman, B. C. Gates, *Dalton Trans.* **2003**, 3303–3318; b) B. C. Gates, *Chem. Rev.* **1995**, *95*, 511–522; c) H. H. Lamb, B. C. Gates, H. Knözinger, *Angew. Chem. Int. Ed. Engl.* **1988**, *27*, 1127–1144; *Angew. Chem.* **1988**, *100*, 1162–1180; d) A. Kulkarni, R. J. Lobo-Lapidus, B. C. Gates, *Chem. Commun.* **2010**, *46*, 5997–6015; e) P. Serna, B. C. Gates, *Accounts Chem. Res.* **2014**, *47*, 2612–2620; f) Z. Wu, G. Hu, D.-e. Jiang, D. R. Mullins, Q.-F. Zhang, L. F. Allard, L.-S. Wang, S. H. Overbury, *Nano Lett.* **2016**, *16*, 6560–6567; g) X. Nie, H. Qian, Q. Ge, H. Xu, R. Jin, *ACS Nano* **2012**, *6*, 6014–6022; h) X. Nie, C. Zeng, X. Ma, H. Qian, Q. Ge, H. Xu, R. Jin, *Nanoscale* **2013**, *5*, 5912–5918.

[12] a) S. Gaur, J. T. Miller, D. Stellwagen, A. Sanampudi, C. S. S. R. Kumar, J. J. Spivey, *Phys. Chem. Chem. Phys.* **2012**, *14*, 1627–1634; b) M. S. Nashner, A. I. Frenkel, D. L. Adler, J. R. Shapley, R. G. Nuzzo, *J. Am. Chem. Soc.* **1997**, *119*, 7760–7771; c) B. D. Chandler, A. B. Schabel, C. F. Blanford, L. H. Pignolet, *J. Catal.* **1999**, *187*, 367–384.

[13] a) S. Yamazoe, T. Yoskamtorn, S. Takano, S. Yadnum, J. Limtrakul, T. Tsukuda, *Chem. Rec.* **2016**, *16*, 2338–2348; b) T. Yoskamtorn, S. Yamazoe, R. Takahata, J.-i. Nishigaki, A. Thivasasith, J. Limtrakul, T. Tsukuda, *ACS Catal.* **2014**, *4*, 3696–3700; c) S. Xie, H. Tsunoyama, W. Kurashige, Y. Negishi, T. Tsukuda, *ACS Catal.* **2012**, *2*, 1519–1523; d) M. S. Bootharaju, R. Dey, L. E. Gevers, M. N. Hedhili, J.-M. Basset, O. M. Bakr, *J. Am. Chem. Soc.* **2016**, *138*, 13770–13773; e) R. R. Nasaruddin, T. Chen, N. Yan, J. Xie, *Coord. Chem. Rev.* **2018**, *368*, 60–79; f) J. Fang, J. Li, B. Zhang, X. Yuan, H. Asakura, T. Tanaka, K. Teramura, J. Xie, N. Yan, *Nanoscale* **2015**, *7*, 6325–6333; g) C. García, S. Pollitt, M. van der Linden, V. Truttmann, C. Rameshan, R. Rameshan, E. Pittenauer, P. Allmaier, P. Kregsamer, M. Stöger-Pollach, N. Barrabés, G. Rupprechter, *Catal. Today* **2019**, *336*, 174–185; h) Z. Wu, D.-e. Jiang, A. K. P. Mann, D. R. Mullins, Z.-A. Qiao, L. F. Allard, C. Zeng, R. Jin, S. H. Overbury, *J. Am. Chem. Soc.* **2014**, *136*, 6111–6122; i) X. Du, R. Jin, *ACS Nano* **2019**, *13*, 7383–7387; j) C. Vriamont, T. Haynes, E. McCague-Murphy, F. Pennetreau, O. Riant, S. Hermans, *J. Catal.* **2015**, *329*, 389–400.

[14] a) M. A. MacDonald, D. M. Chevrier, P. Zhang, H. Qian, R. Jin, *J. Phys. Chem. C* **2011**, *115*, 15282–15287; b) H. Qian, R. Jin, *Nano Lett.* **2009**, *9*, 4083–4087; c) B. Zhang, A. Sels, G. Salassa, S. Pollitt, V. Truttmann, C. Rameshan, J. Llorca, W. Olszewski, G. Rupprechter, T. Bürgi, N. Barrabes, *ChemCatChem* **2018**, *10*, 5372–5376.

[15] a) M. Turner, V. B. Golovko, O. P. H. Vaughan, P. Abdulkin, A. Berenguer-Murcia, M. S. Tikhov, B. F. G. Johnson, R. M. Lambert, *Nature* **2008**, *454*, 981–983; b) D. P. Anderson, J. F. Alvino, A. Gentleman, H. Al Qahtani, L. Thomsen, M. I. J. Polson, G. F. Metha, V. B. Golovko, G. G. Andersson, *Phys. Chem. Chem. Phys.* **2013**, *15*, 3917–3929; c) D. P. Anderson, R. H. Adnan, J. F. Alvino, O. Shipper, B. Donoeva, J. Y. Ruzicka, H. Al Qahtani, H. H. Harris, B. Cowie, J. B. Aitken, V. B. Golovko, G. F. Metha, G. G. Andersson, *Phys. Chem. Chem. Phys.* **2013**, *15*, 14806–14813; d) G. G. Andersson, V. B. Golovko, J. F. Alvino, T. Bennett, O. Wrede, S. M. Mejia, H. S. Al Qahtani, R. Adnan, N. Gunby, D. P. Anderson, G. F. Metha, *J. Chem. Phys.* **2014**, *141*, 014702; e) Y. Liu, H. Tsunoyama, T. Akita, T. Tsukuda, *J. Phys. Chem. C* **2009**, *113*, 13457–13461.

[16] F. Wen, U. Englert, B. Gutrath, U. Simon, *Eur. J. Inorg. Chem.* **2008**, 106–111.

[17] a) M. Cargnello, C. Gentilini, T. Montini, E. Fonda, S. Mehraeen, M. Chi, M. Herrera-Collado, N. D. Browning, S. Polizzi, L. Pasquato, P. Fornasiero, *Chem. Mater.* **2010**, *22*, 4335–4345; b) A. M. Abdel-Mageed, G. Kučerová, J. Bansmann, R. J. Behm, *ACS Catal.* **2017**, *7*, 6471–6484.

[18] B. Donoeva, N. Masoud, P. E. de Jongh, *ACS Catal.* **2017**, *7*, 4581–4591.

[19] D. A. Pichugina, N. E. Kuz'menko, A. F. Shestakov, *Russ. Chem. Rev.* **2015**, *84*, 1114–1144.

[20] Z. Swiatkowska-Warkocka, A. Pyatenko, F. Krok, B. R. Jany, M. Marszalek, *Sci. Rep.* **2015**, *5*, 9849.

[21] R. Psaro, R. Ugo, G. M. Zanderighi, B. Besson, A. K. Smith, J. M. Basset, *J. Organomet. Chem.* **1981**, *213*, 215–247.

[22] a) A. I. Frenkel, C. W. Hills, R. G. Nuzzo, *J. Phys. Chem. B* **2001**, *105*, 12689–12703; b) N. S. Marinkovic, K. Sasaki, R. R. Adzic, *Zast. Mater.* **2016**, *57*, 101–109; c) N. S. Marinkovic, K. Sasaki, R. R. Adzic, *J. Electrochem. Soc.* **2018**, *165*, 3222–3230.

[23] J. T. Miller, A. J. Kropf, Y. Zha, J. R. Regalbuto, L. Delannoy, C. Louis, E. Bus, J. A. van Bokhoven, *J. Catal.* **2006**, *240*, 222–234.

[24] J. Timoshenko, A. Halder, B. Yang, S. Seifert, M. J. Pellin, S. Vajda, A. I. Frenkel, *J. Phys. Chem. C* **2018**, *122*, 21686–21693.

[25] a) J. A. Farmer, C. T. Campbell, *Science* **2010**, *329*, 933; b) S. L. Hemmingson, T. E. James, G. M. Feeley, A. M. Tilson, C. T. Campbell, *J. Phys. Chem. C* **2016**, *120*, 12113–12124; c) S. Tosoni, G. Pacchioni, *J. Phys. Chem. C* **2017**, *121*, 28328–28338.

[26] a) T. R. Eaton, A. M. Boston, A. B. Thompson, K. A. Gray, J. M. Notestein, *ChemCatChem* **2014**, *6*, 3215–3222; b) N. E. Thornburg, S. L. Nauert, A. B. Thompson, J. M. Notestein, *ACS Catal.* **2016**, *6*, 6124–6134; c) Y. Wang, F. Wang, Q. Song, Q. Xin, S. Xu, J. Xu, *J. Am. Chem. Soc.* **2013**, *135*, 1506–1515.

[27] a) N. A. Deskins, R. Rousseau, M. Dupuis, *J. Phys. Chem. C* **2009**, *113*, 14583–14586; b) F. R. Negreiros, M. F. Camellone, S. Fabris, *J. Phys. Chem. C* **2015**, *119*, 21567–21573.

[28] a) L.-W. Guo, P.-P. Du, X.-P. Fu, C. Ma, J. Zeng, R. Si, Y.-Y. Huang, C.-J. Jia, Y.-W. Zhang, C.-H. Yan, *Nat. Commun.* **2016**, *7*, 13481; b) T. Fujitani, I. Nakamura, *Angew. Chem. Int. Ed.* **2011**, *50*, 10144–10147; *Angew. Chem.* **2011**, *123*, 10326–10329; c) J. Saavedra, H. A. Doan, C. J. Pursell, L. C. Grabow, B. D. Chandler, *Science* **2014**, *345*, 1599; d) N. Lopez, T. V. W. Janssens, B. S. Clausen, Y. Xu, M. Mavrikakis, T. Bligaard, J. K. Nørskov, *J. Catal.* **2004**, *223*, 232–235; e) M. M. Schubert, S. Hackenberg, A. C. van Veen, M. Muhler, V. Plzak, R. J. Behm, *J. Catal.* **2001**, *197*, 113–122.

[29] a) W.-S. Lee, R. Zhang, M. C. Akatay, C. D. Baertsch, E. A. Stach, F. H. Ribeiro, W. N. Delgass, *ACS Catal.* **2011**, *1*, 1327–1330; b) V. Aguilar-Guerrero, R. J. Lobo-Lapidus, B. C. Gates, *J. Phys. Chem. C* **2009**, *113*, 3259–3269.

[30] a) J.-X. Liu, I. A. W. Filot, Y. Su, B. Zijlstra, E. J. M. Hensen, *J. Phys. Chem. C* **2018**, *122*, 8327–8340; b) A. Nijamudheen, A. Datta, *J. Mol. Struct. THEOCHEM* **2010**, *945*, 93–96.